Applied Energy 250 (2019) 558–567

Contents lists available at ScienceDirect

Applied Energy

journal homepage: www.elsevier.com/locate/apenergy

Integration of reversible solid oxide cells with methane synthesis (ReSOC-MS) in grid stabilization: A dynamic investigation

Bin Chen[a,b,d], Yashar S. Hajimolana[b,c,*], Vikrant Venkataraman[b], Meng Ni[d,*], P.V. Aravind[b]

[a] Institute of Deep Earth Sciences and Green Energy, Shenzhen University, Shenzhen 518060, China
[b] Process and Energy Department, Delft University of Technology, Leeghwaterstraat 44, CA Delft 2628, the Netherlands
[c] Department of Thermal and Fluid Engineering, Faculty of Engineering Technology, University of Twente, Drienerlolaan 5, 7500 AE Enschede, the Netherlands
[d] Building Energy Research Group, Department of Building and Real Estate, The Hong Kong Polytechnic University, Hung Hom, Kowloon, Hong Kong, China

HIGHLIGHTS

- A novel reversible solid oxide fuel cells system for grid stabilization.
- A two-staged methanation subsystem utilizes the H_2 from SOEC operating and CO_2.
- A control strategy of 7 modes (**M1**–**M7**) operation is proposed.
- **M2** and **M6** are optimal in terms of energy efficiency and system risk.
- Dynamic simulations are conducted to investigate the system.

ARTICLE INFO

Keywords:
Reversible solid oxide cell
Methane synthesis
Grid stabilization
Hydrogen storage
Dynamic simulation
Power control strategy
Power-to-X

ABSTRACT

The power to gas concept is promising for the next generation of electrochemical energy storage and grid stabilization technologies. The fuel produced from electricity-driven fuel production can be an efficient energy carrier for excessive grid power. Here, a reversible solid oxide cell(s) system integrated with methane synthesis (ReSOC-MS) is proposed for the grid stabilization application at Mega Watts class. CH_4 can be synthesized at grid surplus conditions and can be a transportation friendly energy carrier. A control strategy is proposed for this combined system, based on the grid state and H_2 tank state of the system for the normal solid oxide fuel cell (SOFC) mode and solid oxide electrolysis cell (SOEC) mode. Simulation results of these two operational modes demonstrate that the ReSOC-MS can achieve 85.34% power to gas efficiency in SOEC mode and 46.95% gas to power efficiency in SOFC mode. Dynamic simulations of stepping grid state for 5000 s operation show that the power to gas efficiency can be higher than 70%, thereby successfully demonstrating the capability of grid-balancing and methane production.

1. Introduction

Alternative sustainable energy sources are urgently required to limit global warming temperatures below 1.5 °C, in order to avoid environmental degradation. Renewable energy sources (RESs) such as wind, tidal and solar energy can provide the needed power in an eco-friendly way [1]. However, RESs are usually intermittent, unstable and seasonal in nature. These characteristics make the integration of RESs into the grid more challenging and thus there is a need for integrating energy storage technologies in order to balance the power grids. Grid energy storage technologies can be categorized into electrochemical methods (such as batteries, capacitors), mechanical methods (such as compressed air, flywheel) and thermal storage (such as Phase change materials) [2]. Some of the desired characteristics of energy storage technologies are: high roundtrip efficiency, low capital cost and fast response [3]. Reversible Solid Oxide Cell (ReSOC) system is a promising technology which can effectively turn surplus power into H_2, CO and O_2 (electrolysis mode) and produce power by the reverse process (fuel cell mode) [4]. The system that can operate in both solid oxide electrolyser (SOEC) and solid oxide fuel cell (SOFC) mode potentially allows the

* Corresponding authors at: Department of Thermal and Fluid Engineering, Faculty of Engineering Technology, University of Twente, Drienerlolaan 5, 7500 AE Enschede, the Netherlands (Y.S. Hajimolana). Department of Building and Real Estate, The Hong Kong Polytechnic University, Hung Hom, Kowloon, Hong Kong, China (M. Ni).
E-mail addresses: s.hajimolana@utwente.nl (Y.S. Hajimolana), bsmengni@polyu.edu.hk (M. Ni).

https://doi.org/10.1016/j.apenergy.2019.04.162
Received 20 November 2018; Received in revised form 28 April 2019; Accepted 29 April 2019
Available online 10 May 2019
0306-2619/

reduction of complexity, carbon footprint and cost of the Power-to-X plant, unifying hydrogen production and utilization in the same device. In this regenerative operating mode, SOFC/SOEC system is able to better utilize and support the electricity grid. One of the main obstacles in using ReSOC for grid stabilization is the H_2 storage during the SOEC operational mode. Finding a cost-effective method of storing H_2 remains a difficult challenge [5]. An alternative strategy is the further conversion of H_2 produced in the SOEC mode to methane, methanol and other hydrocarbons that are easier for storage and transportation [6].

Jensen et al. proposed a methane synthesis system by internal reforming of H_2 and CO in ReSOC, followed by underground storage of pressurized CH_4. Analysis of the system reveals that ReSOC is thermodynamically and economically benign for high-efficiency large scale electricity storage [7]. Wendel et. al. studied the thermal management and operating conditions for a pressurized ReSOC system with internal methane production (CO methanation), finding a 70% roundtrip efficiency at elevated operating stack pressure (20 bar) [8]. Tinoco et al. investigated a dynamic simulation approach for catalytical H_2 to methanol process at 80 bar, 533 K, at which the H_2 can react with CO_2 to produce liquid methanol. This process is based on a CO_2/H_2 co-electrolysis (SOEC mode) and a single-step methanol reactor [9].

Compared to the CO methanation mentioned above, CO_2 methanation is considered as a more attractive option since it can serve to recycle the CO_2 from various carbon capture and storage (CCS) technologies, thereby leading to carbon dioxide utilisation. By this, CO_2 emission can be alleviated by increasing the penetration of as-synthesized sustainable methane into the fuel supply chain. Besides, CO_2 methanation can also be operated at moderate conditions in well-commercialized large scale methanators, which use low-cost Ni-based catalysts, e.g. the adiabatic fixed bed process system from Lurgi GmbH and TREMP™, cooled fixed-bed from Linde, and other fluidized-bed methanation processes [10].

Therefore, this paper proposes a system with the reversible solid oxide cell subsystem and the methane synthesis subsystem (ReSOC-MS) for the grid power stabilization. In the SOEC mode, the ReSOC-MS system can utilize surplus electricity from the grid to produce H_2, which, optionally, can be further used for CO_2 methanation. Thereby assisting in grid electricity storage in the form of chemicals. In the SOFC mode, ReSOC-MS generates electricity from stored H_2 which is then supplied to the grid. To simplify the system, the two subsystems are thermally coupled to recycle waste heat and to regenerate steam so that external supply of steam and heat can be spared to a great extent. Further, a preliminary control strategy for the combined system is proposed to ensure the stabilization of the grid and the system.

2. Model development

2.1. Overview of the system

The ReSOC-MS system consists of two sub-systems as depicted in Fig. 1: the ReSOC subsystem and the methanation subsystem, connected by the H_2 supply stream (***S16***) and the water recycle stream (***S18***). The grid is linked to the ReSOC subsystem by the electricity output (W_{elec_EC} in the unit of MW) during the SOEC operational mode. Thus when there is a surplus of electricity in the grid, it is stored by the ReSOC subsystem by working in SOEC operational mode. Alternatively, during electricity shortage, the grid is connected to the ReSOC by the electricity input (W_{elec_FC}), thus the ReSOC operates in SOFC mode to generate the required electricity needed for the grid. A PID controller is employed to regulate the power of ReSOC by varying the current density.

Steam electrolysis at 600 °C for producing H_2 and O_2 from steam at SOEC mode:

$$2H_2O = O_2 + 2H_2 \quad \Delta H = 493 \ \text{kJ mol}^{-1} \tag{1}$$

In order to accommodate the surplus electricity from the fluctuating grid, the stored H_2 in the tank may exceed its capacity, therefore, it needs to be further transferred to the methane synthesis subsystem where the Sabatier reaction takes place:

$$CO_2 + 4H_2 = CH_4 + 2H_2O \quad \Delta H = -164 \ \text{kJ mol}^{-1} \tag{2}$$

The methane synthesis subsystem consists of two Sabatier reactors with inter-stage cooling. The H_2 from the tank will be firstly adiabatically compressed to the working pressure (10 bar, ***S17***), and mixed with the compressed CO_2 (***S19***) source and the recycled product gas (***S26***). The inlet gas temperature of the first stage Methanator1 is fixed at 250 °C by means of gas recycle from Condenser ***C2***. To improve the conversion of CO_2 and H_2 to CH_4, the steam generator (***SG1***, an evaporative water intercooler) is used to lower down the temperature of ***S21*** to 400 °C, while the steam (***S22***) generated from the evaporation of water can be used as the reactant of the electrolysis process ongoing at the ReSOC (SOEC mode). The CH_4 is further synthesized in the Methanator2 with the waste heat of the off-gas (***S23***) recuperated by the steam generator (***SG2***), meanwhile yielding steam (***S25***). Finally, the condenser ***C2*** will condense the steam contained in ***S24*** to liquid water (***S18***) and then the CH_4 rich gas (***S27***) is stored with 10% recycled to Methanator1.

As said, the control bus component is responsible for the real-time control of gas streams flux so that the ReSOC-MS system can switch between SOFC mode and SOEC mode. To achieve this, the system state should be defined by two descriptive variables: the grid state S_e and the H_2 tank state S_{H_2}. The dimensionless S_e represents the grid electricity surplus or shortage, normalized to 5 MW ($E_{nominal}$) from −1.0 to 1.0 in the tentative application scenario:

$$S_e = \frac{-W_{elec\_EC}}{E_{nominal}} or \frac{W_{elec\_FC}}{E_{nominal}} \tag{3}$$

The other state variable is S_{H_2}, which represents the filling degree of the H_2 tank:

$$S_{H_2} = \frac{Volume \ \ of \ \ H_2 \ \ stored}{Maximum \ \ volume \ \ of \ \ H_2 \ \ tank} \tag{4}$$

Evidently, S_e is negative when the grid is subject to the electricity demand, which is less than the supply, implying that excess electricity needs to be stored via electrolysis process (SOEC mode). When S_e is larger than zero, the ReSOC would be operated at SOFC mode to compensate for the electricity shortage, thus securing the grid balance. It is assumed than the upper bound of fluctuating renewable power plant grid (W_{elec_EC} or W_{elec_FC}) is less than E_nominal in all scenarios, so that the intermittence of the grid can be mimicked by the changing S_e within ± 1 as a simplification. The other state variable is S_{H_2}, representing the filling degree of the H_2 tank from 0% to 100%. A state-dependent control strategy based on these two state variables is implemented into the control bus to regulate three pipe opening valves (***V1***-***V3***). The details of the control strategy are provided in Section 2.4.

To investigate the efficiency and dynamic operation of the proposed system, the system model is developed in the dynamic simulation Platform *OpenModelica* based on the process modelling language Modelica. Using the built-in basic blocks of *OpenModelica*, models for system components are developed and connected, with 5590 variables to be solved using the DASSL dynamic solver with a 0.02 s time step. The computational time for a simulated 5000 s operation is less than 5 min. The following section will introduce the details of component model development.

2.2. ReSOC subsystem model

The ReSOC subsystem utilizes excess electricity (W_{elec_EC}) from the grid to electrolyze the steam-rich stream (***S9***, the mixture of ***S6***, ***S22***, ***S25*** and ***S28***) to produce H_2 and O_2. The electricity-powered steam generator (***SG3***) is responsible for supplying additional steam to adjust the fraction of steam in ***S9*** before entering the stack. The fuel stream

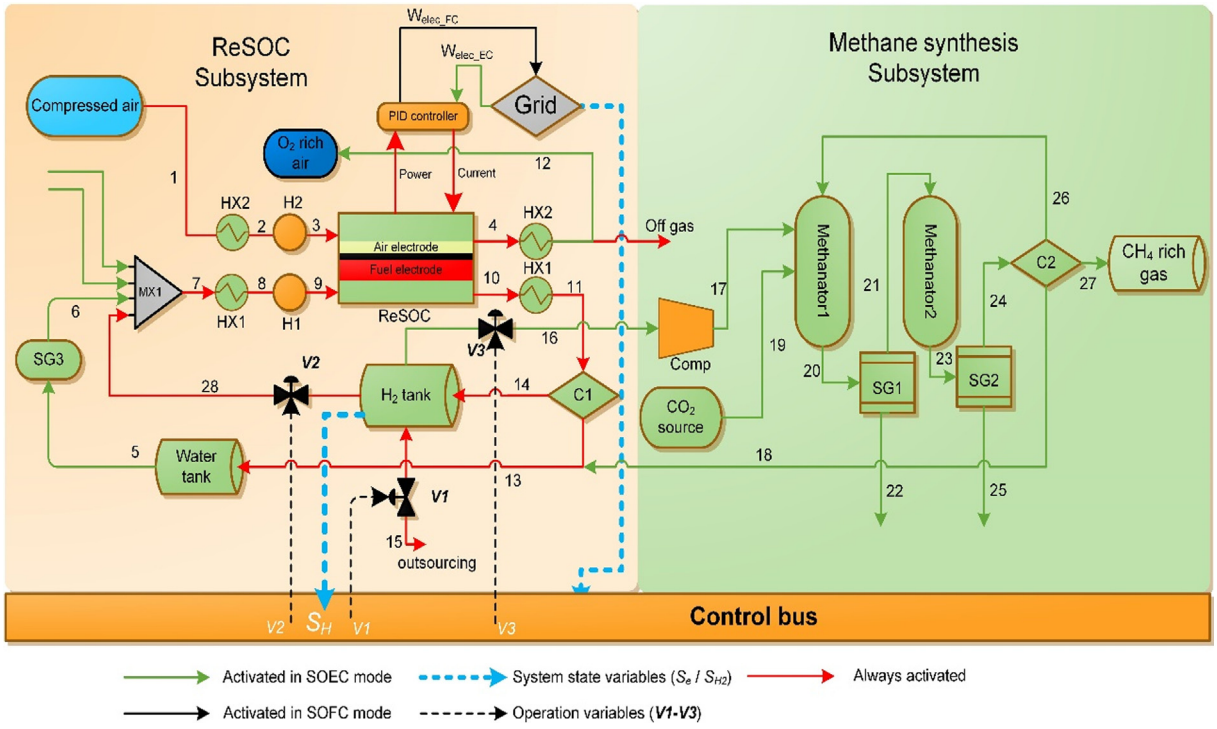

Fig. 1. The overall system schematic of the ReSOC-MS system.

(***S7***) is heated up to the operating temperature (600 °C) by heat exchanger ***HX1*** and heater ***H1***. The produced H_2 by ReSOC (SOEC mode) in ***S10*** is stored in the H_2 tank via ***S14***, after heat recuperation (at ***HX1***) and unused steam splitting at Condenser (***C1***). The stored H_2 can be utilized by the ReSOC via ***S28*** to generate electricity, thus avoiding the grid shortage when the ReSOC operates at SOFC mode (reserved Eq. (1)). The storage of H_2 at the storage tank is assumed to be ideal, without thermal loss/leakage during the operation. Low-pressure absorption method, e.g. using metal hydride is assumed for this H_2 storage tank [11,12], mainly for two reasons: first, the ReSOC stack is intended to operate under ambient pressure as a high-pressure operation will inevitably bring complexity to the ReSOC subsystem, although it is thermodynamically beneficial in terms of energy efficiency. Second in the reversible ReSOC system, compressed storage of H_2 will require additional compression/expansion work for H_2 implying significant energy loss. The H_2 balance at the H_2 storage tank is controlled by three valves (***V1***, ***V2*** and ***V3***), which are regulated by the control bus. It should be noted that ***V1*** is a bidirectional valve for H_2 export/replenishment, assuming that its opening can be two-way, i.e. −1 to 0 for exporting and 0 to +1 for replenishing, to avoid overfilling and complete draining of the H_2 storage tank.

On the air electrode side, the air flow rate is 0.5 mol s^{-1} in SOEC mode as the carrying gas supplied by the compressed air tank. In SOFC mode, the air flow is proportional to S_e, i.e. $10 \cdot S_e$ mol s^{-1} so that the utilization of the oxygen is controlled at 30%. The off gas from the air channel in SOEC mode is oxygen-rich, thus is stored in the O_2 rich gas storage tank as a chemical product. Heat exchanger ***HX2*** and Heater ***H2*** are also designed to control the inlet temperature of the air flow stream (***S3***) to be consistent with that of the inlet fuel flow of the ReSOC. The ***HX1*** and ***HX2*** are counter-flow type with the effectiveness factor at 0.85. The effectiveness factor is defined as the ratio of the actual heat exchange rate to the theoretical maximum heat exchange rate between the two fluid streams [13]. Table 1 summarizes the operating parameters for the blocks in the ReSOC subsystem.

A zero-dimensional dynamic model for the stack is developed based on transfer functions of the partial pressure of participating gas species. Ohmic loss, activation loss and concentration loss are all taken into consideration in this model. The transfer function based zero-dimensional dynamic model has advantages in integrating with system control algorithms, compared to traditional numerical models (e.g. Finite Element Method, Finite Volume Method) that require time-consuming computational solving of partial differential equations. Fig. S1 shows the mathematical model of the stack with three input ports and three output ports interfaced to external components in the ReSOC system [14,15]. The first input port is the operating current density instructed by the PID controller, and the other two are the fuel inflow stream and air inflow stream. The power output port is connected to the PID controller for the current control, while the fuel output and air output port are connected to other components for further heat recovery and gas processing as shown in Fig. 1. The grid state parameters (electricity input W_{elec_EC} to ReSOC; or W_{elec_FC} output from ReSOC) are used as the "setpoint" of the PID controller. The "error value" is the difference between stack power and the "setpoint". The operating current of the stack is the manipulated variable by the controller. The controller will fail when the grid power is beyond the power capacity of the stack,

Table 1
The nominal operation conditions of auxiliary blocks of the ReSOC subsystem.

Blocks	Parameters and values
Heat exchanger (***HX1–2***)	Effectiveness: 0.85
Heaters (***H1–2***)	Outlet temperature: 600 °C
Steam generator (***SG3***)	Outlet temperature: 100 °C
Compressed air	Flowrate: 0.5 mol s^{-1} at SOEC; $10 \cdot S_e$ mol s^{-1} at SOFC; Pressure: slightly[a] > 1 bar
Water tank	25 °C, 1 bar
H_2 tank	25 °C, 1 bar, capacity: 6000 mol H_2
Maximum valve flowrate for ***V2*** and ***V3***	55 mol s^{-1}; 20 mol s^{-1}
Condenser (***C1***)	Condensing temperature: 100 °C
PID controller	kp = 0.0001; ki = 1; kd = 1

[a] Ideally assumed to be 1 bar in simulation, while in practical, the outlet pressure of the compressed air tank should be calibrated at slightly > 1 bar to offset the pressure loss.

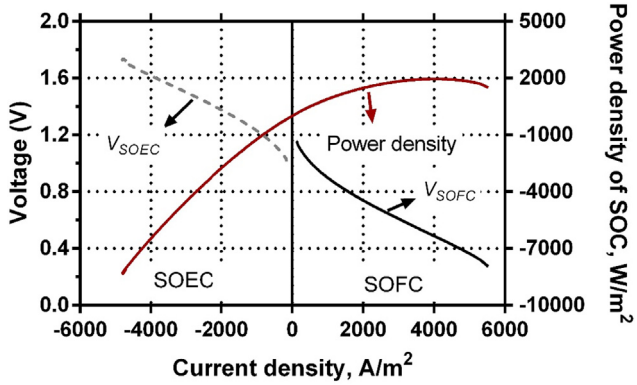

Fig. 2. The simulated ReSOC performance in dual modes: SOEC(left) and SOFC(right); Inlet fuel gas: 97% H_2, 3% H_2O at SOFC and 95% H_2O, 5% H_2 at SOEC; Air electrode: air; 600 °C.

which is defined as $W_{elec\_FC} > 1.28$ MW and $W_{elec\_EC} > 6.4$ MW. The PID coefficients *kp*, *ki* and *kd*, representing the proportional, integral and derivate gains, were manually tuned to ensure that the output power from the stack can respond to the grid state without oscillating, referred to Table 1.

The following are assumptions used in this ReSOC model:

1. All gas flows behave as ideal gases.
2. The temperature of the ReSOC is set as the inlet temperature 600 °C.
3. The gas channel is a fixed control volume and the flow is assumed to be plug flow.
4. The Nernst equation is applied to calculate the open circuit voltage.
5. A First-order transfer function is used to describe the gas composition change during the process.
6. The two flows of channels are choked at orifices of outlets [16].

Using the models and assumptions mentioned above, the final zero dimensional dynamic ReSOC stack model is implemented with other components to form the ReSOC subsystem. Fig. 2 shows the simulated current-voltage curve of a single cell of the ReSOC stack, that is a conservative representative of current solid oxide cell performance at intermediate temperature (600 °C), of which the maximum power density ranges from 0.2 W cm^{-2} to 1.58 W cm^{-2} [17]. For simplicity, the single cell performance is extrapolated to represent every cell in the whole stack. The discontinuity of the current curve between the SOEC mode and SOFC mode arises from the different inlet fuel gas compositions.

2.3. Methanation subsystem

The methanation subsystem is responsible for the synthesis of methane using the H_2 stored in the storage tank (25 °C, 1 bar), which is produced by the ReSOC subsystem at the SOEC mode. The process is based on the concept of CO_2 methanation (Sabatier reaction) in two identical adiabatic fixed-bed methanators (Methanator1 and Methanator2) with inter-stage cooling. The process proposed here is from the exemplary 3-staged TREMP methanation process developed by Haldor Topsøe™ [10].

The H_2 sources from the H_2 storage tank is firstly adiabatically compressed to the operating pressure (10 bar, ***S17***), and then mixed with the compressed CO_2 (***S19***) source and the recycled product gas (***S26***). The inlet gas temperature of the first stage Methanator1 is fixed at 250 °C by means of gas recycle from Condenser ***C2***. To improve the conversion of CO_2 and H_2 to CH_4, the steam generator (***SG1***, an evaporative water intercooler) is used to lower down the temperature of ***S21*** to 400 °C, while the steam (***S22***) generated from the evaporation of water can be used as the reactant for the electrolysis process at the

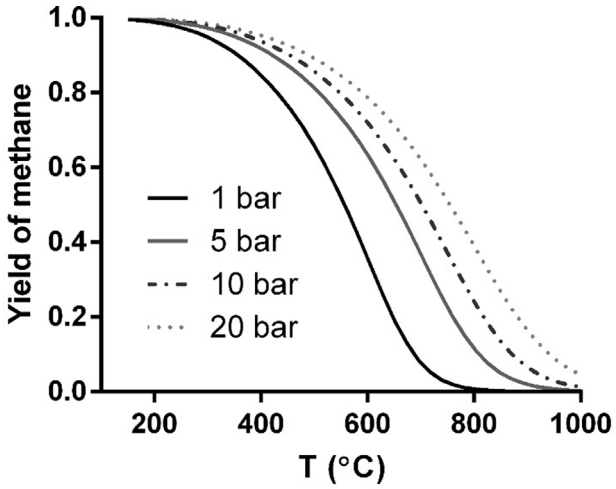

Fig. 3. Yield of methane at thermodynamic equilibrium for stoichiometric feed gas composition (CO_2 = 20%, H_2 = 80%) [10].

ReSOC (SOEC case). The CH_4 is to be furtherly synthesized in the Methanator2 utilising the waste heat of the off-gas (***S23***) recuperated by the steam generator (***SG2***), meanwhile yielding steam (***S25***). Finally, the steam contained in ***S24*** is condensed to liquid water (***S18***) by the condenser ***C2*** and the CH_4 rich gas (***S27***) is stored, with 10% recycled back to Methanator1.

The main advantage of the methanation process proposed in this study is that the byproduct steam can be recycled to the ReSOC for use as the reactant for H_2O_g electrolysis, and that heat can be recovered from the methanation process at the same time. The main reaction occurring in two methanators is the so-called CO_2 methanation reaction (see Eq. (2)). As it is an endothermic reaction, a higher yield of CH_4 is favoured at a lower temperature, as shown in Fig. 3 and the theoretical equilibrium yield of CH_4 approaches 1 when the temperature is reduced. Therefore, the feed gas temperature of Methantor1 is controlled at 250 °C to thermodynamically facilitate the CH_4 production. Preheating the H_2 stream and recycling 10% of the outlet gas flow of Methanator2 at the condenser (***C2***) are the two measures to control the inlet temperature of Methanator1. Before Methanator2, ***SG1*** is used to cool down the outlet gas of Methanator1 to 400 °C before entering Methanator2. The design parameters for the methanators are summarized in Table 2. The operating parameters for auxiliary components of the methanation subsystem are listed in Table 3.

The mathematical model for CO_2 methanation reactors is based on the kinetics over Ni/Al_2O_3 catalyst, adopted from Koschany's power law equation [22].

$$r = k \cdot \frac{p_{H2}^{nH2}\, p_{CO2}^{nCO2}}{1 + K_{OH}\frac{p_{H_2O}}{p_{H_2}^{1/2}}} \left(1 - \frac{p_{CH_4} p_{H_2O}^2}{p_{H_2}^4 p_{CO_2} K_{eq}}\right) \quad (5)$$

Table 2
Methanator design parameters used in the modelling [18].

Methanator parameters	Value
Working pressure	10 bar
Catalyst type	Ni/Al_2O_3
Catalyst density (ρ_c)	2800 kg mol^{-1}
Bed porosity	0.4
Methanator catalyst loading	3.0 kg
Methanator inner diameter	0.45 m
Methanator length	2.0 m
Space velocity, GSHV (nominal, ***V3*** = 1)	6800 h^{-1} (STP)
Inlet gas composition before mixing with recycled gas	H_2:CO_2 = 4
Inlet gas flowrate before mixing (nominal, ***V3*** = 1)	25 mol s^{-1}
Discretized element number	400

Table 3
The operation parameters of auxiliary blocks of methanation subsystem.

Blocks	Parameters	Value
H_2 source (***S16***)	Temperature, T_{H_2}	25 °C
	Pressure, P_{H_2} [19]	10 bar
	Maximum flowrate, F_{H_2}	20 mol s^{-1}
CO_2 source	Temperature, T_{CO_2}	25 °C
	Pressure, P_{CO_2} [19]	10 bar
	Maximum flowrate, F_{CO_2}	5 mol s^{-1}
Steam generator (***SG1–2***)	Temperature of feed-water	25 °C
	Outlet steam temperature	100 °C
Methanator1	Inlet temperature	250 °C
Methanator2	Inlet temperature [20]	400 °C
Condenser (***C2***)	Recycle ratio	10%
	Outlet temperature at 10 bar [21]	177 °C
Compressor (***COMP***)	Compressing ratio	10
	Isentropic efficiency	85%

which the r represents the volume-based reaction rate of CO_2 methanation in mol (s^{-1} m^{-3}).

A one-dimensional plug-flow model is developed to simulate the reaction process inside the methanator along the flow direction [23]. The radial gradients of temperature, species concentration, heat losses and pressure drop along the flow are neglected. Thus, the spatial-dependent model can calculate the distribution of reaction rates, the temperature of the gas flow T and the gas species concentration c_j.

2.4. Control strategy

As briefly mentioned in Section 2.1, the control strategy implemented in the control bus block is to regulate ReSOC-MS system in switching between SOFC mode and SOEC mode, as well as managing the operation of the methane synthesis subsystem. The control strategy is based on two variables (S_e, S_{H_2}), which maps out the system state space (Fig. 4) that is partitioned to 7 regions, each corresponding to an operation mode (**M1**–**M7**) to improve the control performance. By this, comprehensive control strategies are implemented for incorporating the methanation subsystem with the ReSOC subsystem. Generally, **M1**–**M3** are responsible for subdividing the SOFC case operating when $S_e > 0$. Specifically, **M2** is the optimal mode for SOFC operating as the H_2 used by the SOFC is pre-stored, without the need for external supply of H_2 (e.g. **M1**) which would be more energy-costive. It is rational to activate the methanation process at **M3** to consume H_2 when the filling of H_2 storage tank is close to 100%, also taking into account that the ReSOC too needs H_2 for SOFC operation. On the other hand, **M4**–**M7** are for subdividing SOEC operation when $S_e < 0$. At **M4** and **M5**, the methanation system is designed to be inactive, considering that the stored H_2 is close to depletion. **M6** is deemed as the optimal condition since the filling of H_2 stack can be properly regulated to reduce the risk of brimming by flexibly controlling the H_2 consumption rate to the methanation process (partial activation of methanation by ***V3***). Therefore, the aforementioned 7 modes of operation enables the proper integration of methanation subsystem to the ReSOC subsystem by controlling the openings of three valves of H_2 tank (***V1***, ***V2*** and ***V3***) to regulate the H_2 consumption/production rate, the methanation rate and the export/replenishment of the H_2 from/to the storage tank, respectively. The maximum openings of ***V1***–***V3*** for H_2 flowrate are capped at 25 mol s^{-1}, 55 mol s^{-1} and 20 mol s^{-1}. The strategies are mathematically formulated as:

$$\mathbf{M}(S_e, S_{H_2})=$$

$$\mathbf{M1}: V1 = -1(H_2 replenishing);\ V2 = S_e(SOFC);\ V3 = 0,\ S_{H_2} < 0.125;\ 0 < S_e \le 1$$

$$\mathbf{M2}: V1 = 0;\ V2 = S_e(SOFC);\ V3 = 0,\ 0 \le S_e - 2S_{H_2} + 1;\ 0.125 \le S_{H_2};\ 0 < S_e \le 1$$

$$\mathbf{M3}: V1 = \begin{cases} 0 & S_{H_2} < 1 \\ 1 & S_{H_2} = 1,\ H_2 exporting \end{cases};$$

$$V2 = S_e(SOFC);\ V3 = 2S_{H_2} - S_e - 1(Methanation),\ S_e - 2S_{H_2} + 1 < 0,\ 0 < S_e \le 1$$

$$\mathbf{M4}: V1 = -1(H_2 replenishing);\ V2 = 0.05(SOEC);\ V3 = 0,\ S_{H_2} < 0.125;\ -1 \le S_e \le 0$$

$$\mathbf{M5}: V1 = 0;\ V2 = 0.05(SOEC);\ V3 = 0,\ S_{H_2} \ge 0.125;\ S_e - 4S_{H_2} \ge -2,\ -1 \le S_e \le 0$$

$$\mathbf{M6}: V1 = 0;\ V2 = 0.05(SOEC);\ V3 = S_{H_2} - (S_e + 2)/4(Methanation),\ -4 < S_e - 4S_{H_2} < -2,\ -1 \le S_e \le 0$$

$$\mathbf{M7}: V1 = \begin{cases} 0 & S_{H_2} < 1 \\ 1 & S_{H_2} = 1,\ H_2 exporting \end{cases};\ V2 = 0.05(SOEC);\ V3 = 1(Methanation),\ S_e - 4S_{H_2} \le -4,\ -1 \le S_e \le 0 \quad (6)$$

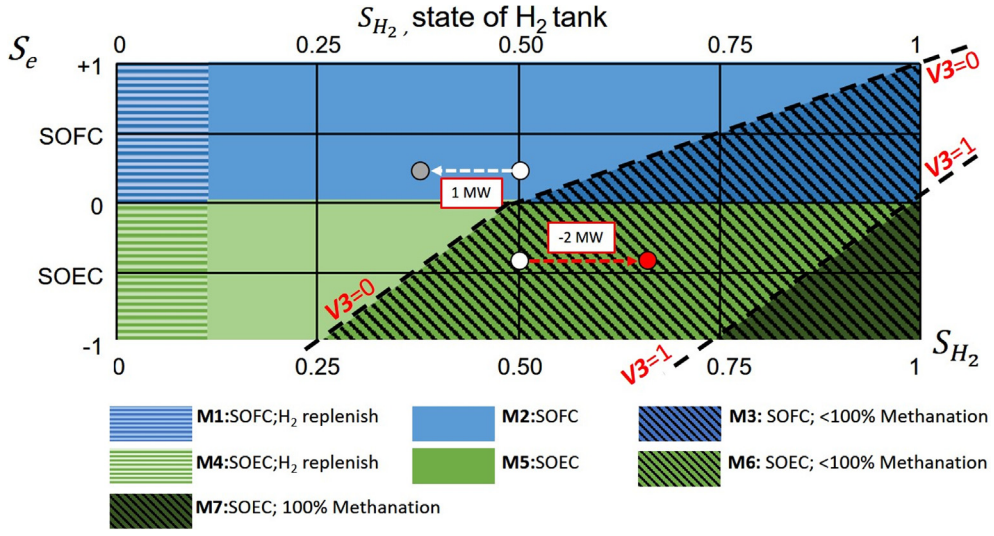

Fig. 4. Control strategy of 7 modes (M1–M7) depending on the system state and the stationary testing case state trajectory at 1 MW and −2 MW grid input.

Using this control strategy, the system can be dynamically operated at fluctuatingS_e, taking the real-time filling state of H_2 tank into consideration. To make it even more clear, Table S2 lists down the operating states of the ReSOC subsystem and the methanation subsystem under those seven modes. The detailed description of each mode is also introduced in the supporting information. To evaluate the robustness of the system, two stationaries S_e cases and two stepping S_e cases are conducted, for both SOEC and SOFC operation modes respectively. This will be discussed in the next section.

3. Results

3.1. Stationary results

Firstly, two stationary cases are conducted to simulate 1000 s operating at SOFC mode and SOEC mode, respectively. The stationary S_e and the initial S_{H_2} for each mode are defined as:

$$\text{SOFC case:} \quad S_e = 0.25,\ S_{H_2} = 0.5 \tag{7}$$

$$\text{SOEC case:} \quad S_e = -0.4,\ S_{H_2} = 0.5 \tag{8}$$

The initial H_2 storage tank state is set at 50% filled ($S_{H_2} = 0.5$). The stack in the SOFC mode ($S_e = 0.25$) generates1 MW of power to the grid respectively, while in the SOEC mode, the stack is required to utilize 2 MW of power from the grid ($S_e = -0.4$) as shown in Fig. 4. The simulated change of (S_e, S_{H_2}) overtime is tracked in Fig. 5. In the SOFC mode, the ***V3*** is always closed as the methanation subsystem is not activated as the value of S_{H_2} is lower than 0.5. Therefore, the operation mode is at **M2** and would not enter **M3**. The S_e is kept at 0.25 since it is pre-defined to be stationary.

In the SOEC mode, the ***V3*** initially delivers H_2 (4 mol s^{-1}) from the H_2 storage tank to the methanation subsystem with its opening set at 0.2. Then, the opening of ***V3*** gradually increases to 0.292 due to the increase of S_{H_2}. The adaptive control of ***V3*** in the case of changing S_{H_2} is realized by the location mapping of (S_e,S_{H_2}) between two boundaries for ***V3*** as it can be seen in the Fig. 4. This strategy is expected to improve the robustness of the energy storage system by enhancement of H_2 consumption via ***V3***. That results in the increase of total methane yield (y_{CH_4}) as observed in Fig. 5c. Finally, the S_{H_2} is only increased to 0.538, indicating that the current system design is competent in balancing MW scale grid in the time scale of thousand seconds. The integration of methanation subsystem and the (S_e,S_{H_2})-dependent methanation rate as designed are proven to be able to mitigate the H_2 storage issue. The initial quick decay of y_{CH_4} before $t \approx 30$ s is because of the quick cooling effect of methanation reaction in the initial stage. The conversion of H_2 at each methanator (noted as $U1$and $U2$) does not change much with the varying of ***V3***, indicating that the methanation capacity of two methanators are sufficient for converting the H_2 input, so that the flow is close to the equilibrium state at the outlet of each methanators. Table 4 gives the performance summary of these two stationary simulation cases.

Fig. 6 compares the energy inflow and outflow for both SOEC and SOFC modes. It should be noted that auxiliary equipment, such as compressors and heaters, need to be powered. Therefore, the total energy input as shown in Fig. 6a (SOEC mode), is the sum of the grid electricity towards the ReSOC and additional electricity input to auxiliary equipment. At 1000 s of SOEC mode, a total of 2.59 GJ power is delivered to the ReSOC system, of which 2 GJ is the excess power from the grid that needs to be balanced and 0.59 GJ is from other sources for the auxiliary components. 77.35% of 2.59 GJ is utilized in the electrolysis process in the ReSOC stack. Regarding the energy output in Fig. 6b, it can be seen that 14.66% of energy is wasted, 56.4% of energy is stored in the CH_4 via methanation and 28.94% of energy is stored in the produced H_2. This conversion efficiency is achieved at 1.44 V which is close to the thermal-neutral voltage (approximately 1.27 V at 600 °C [24]), neglecting the pipeline losses, heat dissipation in gas tanks and

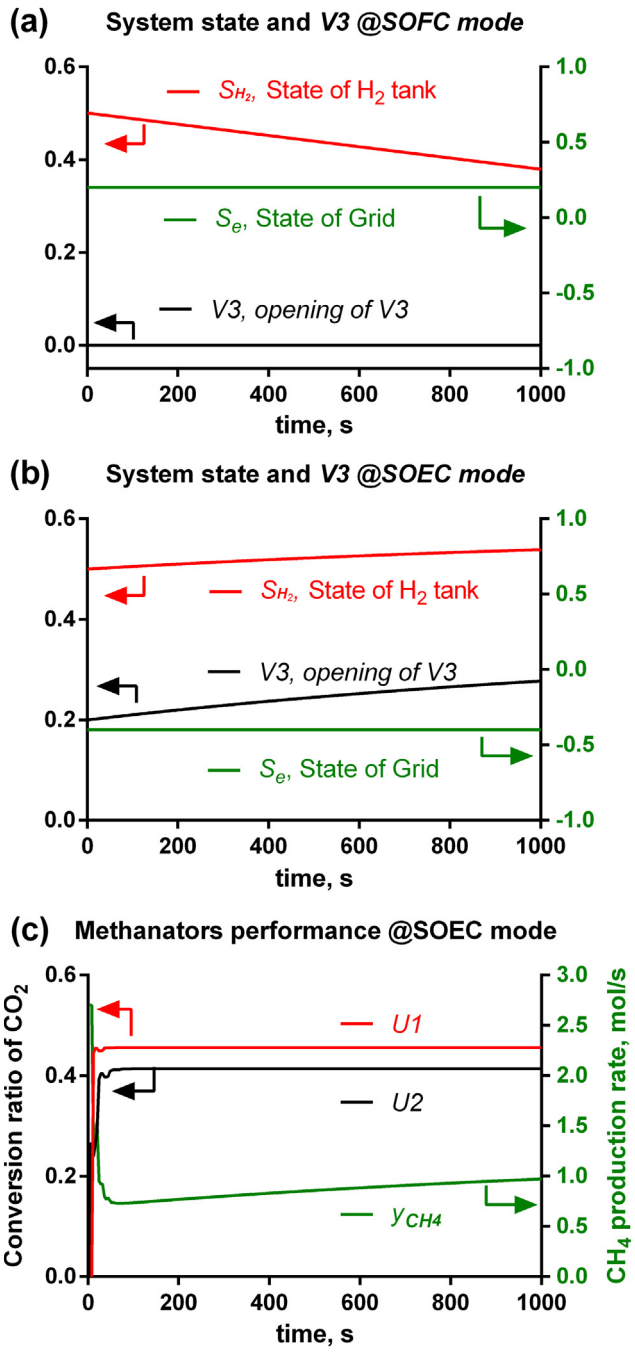

Fig. 5. S_e, S_{H_2} and *V3* in the stationary testing for 1000 s: (a) SOFC mode; (b) SOEC mode and (c) methanator performance at SOEC mode.

heat exchangers. In the SOFC mode (Fig. 6c), 97.63% (2.13 GJ) of the total energy input originates from the High Heating Value (HHV) of the consumed H_2, while a small amount of electricity is needed for other components. Finally, the 46.95% of the total energy input is converted to the grid power (Fig. 6d).

3.2. Dynamic response results

To simulate the grid fluctuations, two stepping electricity conditions for the surplus and shortage are assumed, each lasting for a time span of 5000 s, represented by the stepping grid state variableS_e:

At grid electricity surplus (SOEC case):

Table 4
Summary of stationary performance of the ReSOC-MS at SOFC mode and SOEC case.

Parameters	SOFC case	SOEC case
S_e input	0–1000 s: 0.2 (1 MW)	0–1000 s: −0.4 (−2 MW)
Operation time	1000 s	1000 s
Initial H_2 tank state, S_{H_2}	0.5	0.5
Total power output to grid, W_{g_SOFC}	1000 MJ	−2000 MJ
Total auxiliary power input, W_{aux_SOFC}	50.5 MJ	585.6 MJ
HHV value of H_2 consumption for SOFC, HHV_{H2_SOFC}	2079.5 MJ	Nil
Total HHV production of H_2 and CH_4, HHV_{fuel_SOEC}	Nil	2214 MJ
Average system efficiency	46.95% (gas to power)	85.34% (power to gas)
Operating Voltage of ReSOC, V_{SOC}	0.71 V	1.44 V
Average methane production rate, y_{CH_4}	Nil	0.875 mol s^{-1}

$$S_e = \begin{cases} -0.4,\ t < 2000s\ (W_{elec\_EC} = 2\ \ MW) \\ -0.6,\ 2000s < t < 3000s\ (W_{elec\_EC} = 3\ \ MW) \\ -0.8,\ 3000s < t < 5000s\ (W_{elec\_EC} = 4\ \ MW) \end{cases} \quad (9)$$

At grid electricity shortage (SOFC case):

$$S_e = \begin{cases} 0.06,\ t < 2000s\ (W_{elec\_FC} = 0.3\ \ MW) \\ 0.16,\ 2000s < t < 3000s\ (W_{elec\_FC} = 0.8\ \ MW) \\ 0.26,\ 3000s < t < 5000s\ (W_{W_{elec\_FC}} = 1.3\ \ MW) \end{cases} \quad (10)$$

As schemed in Fig. 7, the grid state valueS_e in the dynamic SOEC mode (red arrows) is initially set at −0.4 for 2000 s, then decreased to −0.6 for 1000 s and is finally kept at −0.8 during the last 2000 s. The corresponding electricity inputs to the ReSOC stack (W_{elec_EC}) for the three steps are 2 MW, 3 MW and 4 MW of power, respectively. Regarding the dynamic SOFC mode, a similar stepping is applied but S_e is changed to 0.06, 0.16 and finally 0.26. Table 5 summarizes the operation conditions and the results of SOEC operational mode. Accordingly, the dynamic operating voltage of the ReSOC is increased from 1.44 V to 1.61 V with nearly no time delay (see Fig. 8). Meanwhile, the H_2 storage tank is gradually filled, with the initial S_{H_2}changing from 0.4 to 0.5 till t = 5000 s (Fig. 9a). The S_{H_2} does not show step-like zigzags at stepping time points of S_e. This is because abrupt changing of H_2 flow (**S14**) into the H_2 storage tank is avoided, due to the opening of valve ***V3*** which is controlled and is proportional to S_e, which is changing stepwise. The stepping change of ***V3*** results in the stepping change of total methane production rate (y_{CH_4}) of the two methanators as seen in Fig. 9b. The conversion rates ($U1$and $U2$) are stable during the whole 5000 s operating. The transient electricity storage rates (electricity to H_2 by electrolysis and electricity to CH_4 by methanation in J/s) are measured separately by the HHV value of H_2 and CH_4 in Fig. 10a. It can be found that the system prefers to store electricity in the form of CH_4 to a higher degree during grid electricity surplus. This is because CH_4 has higher volumetric energy density than H_2. The efficiency of the system (Fig. 10b) decreases at each step of S_e, but still maintains above 0.7, even at 4 MW operating.

For the SOFC mode, the grid state S_e is stepped from 0.06 to 0.26 as pre-designed, represented by the green lines in Fig. 11a. Here, it is assumed that the unbalanced amount of electricity in the SOFC mode is relatively smaller than that in the SOEC mode, because the assumed target grid for the ReSOC-MS system is more often achieved during electricity surplus conditions, i.e. powered by renewable energy resources such as wind or solar power. As it is observed, the S_{H_2} is reduced at different slopes during the three steps. From 0 s to 2000 s, ***V3*** is partially opened to deliver H_2 to the methanation process at the mode **M3** because the storage of H_2 tank is already sufficiently full (S_e > 0.5). As seen in Fig. 11b, the methanation subsystem accordingly yields CH_4 production before 2000 s. Thereafter, the operating mode is

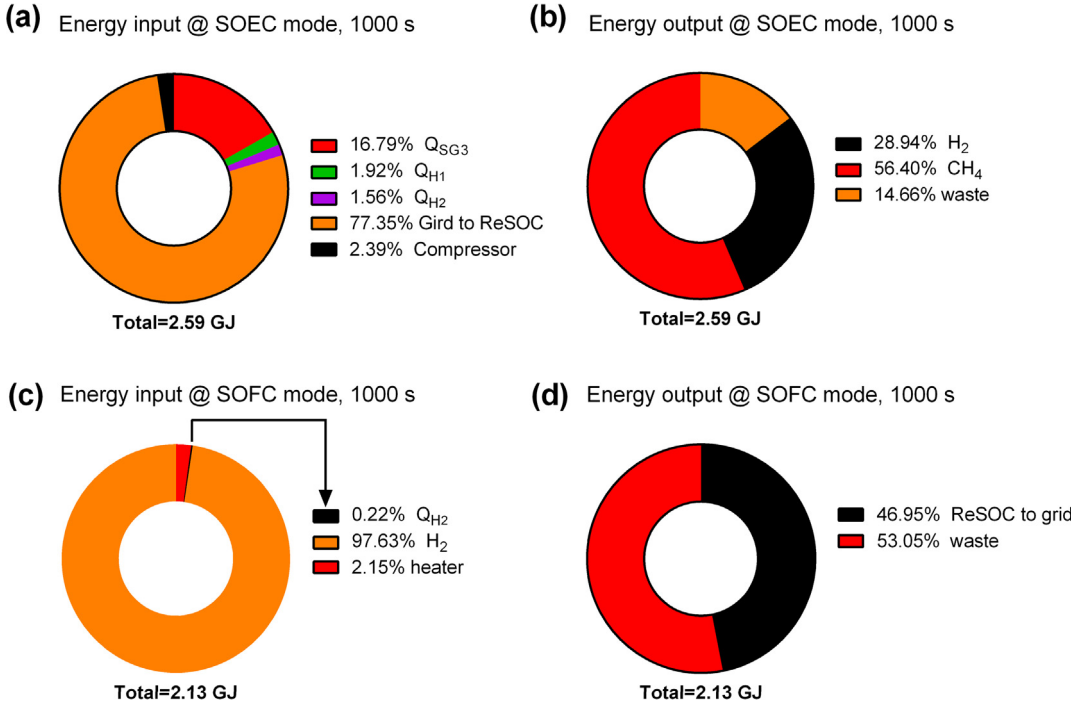

Fig. 6. Accumulative energy incomings and outgoings for the SOEC case (a, b) and SOFC case (c, d) at 1000 s.

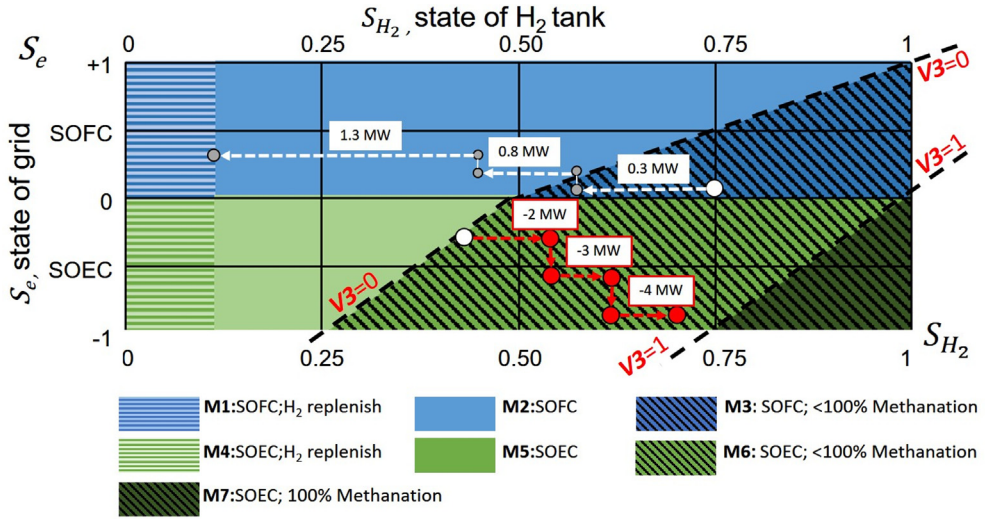

Fig. 7. The dynamic operation testing of SOEC and SOFC mode of the ReSOC-MS system and its system state trajectories (red arrow: SOEC; white arrow: SOFC).

Table 5
Summary of dynamic operation conditions and performance of the ReSOC-MS system in the SOEC case.

Performance parameters	Value
Average methane production rate, y_{CH_4}	2.2326 mol s^{-1}
Average CO_2 conversion ratio	$U1 = 0.456$; $U2 = 0.41$
Operation time	5000 s
Initial H_2 tank state, S_{H_2}	0.4
Stepping S_e input	0–2000 s: −0.4 (−2 MW) 2000–3000 s: −0.6 (−3 MW) 3000–5000 s: −0.8 (−4 MW)
Total HHV production of H_2 and CH_4, HHV_{fuel_SOEC}	13,482 MJ
Total grid electricity input: W_{g_SOEC}	15,000 MJ
Total auxiliary power input, W_{aux_SOEC}	3968.7 MJ
Average system efficiency (power to gas)	71.70%
Operating voltage of ReSOC, V_{SOC}	1.44 V; 1.53 V; 1.61 V
Working temperature of ReSOC, T_{SOC}	600 °C

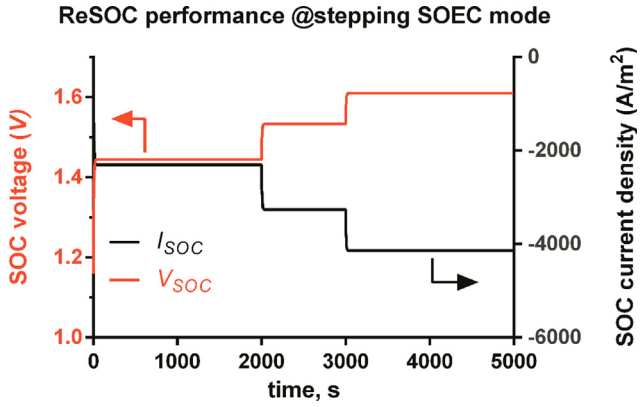

Fig. 8. Dynamic performance of the ReSOC at SOEC mode.

switched from **M3** to **M2**, corresponding to the boundary crossing in Fig. 7 due to the sudden change of S_e. This mode switch resulted in closing of ***V3***, due to which the production of CH_4 is stopped after $t = 2000$ s (see Fig. 11b). After $t = 3000$ s, the decrease in the rate of S_{H_2} is constant until S_{H_2} reaches 0.125 at $t = 4836$ s. After that, the outsourcing mode is triggered (**M1**) that holds the S_{H_2} value at 0.125 (Fig. 11a). The fast responsivity of voltage and current curves of the ReSOC subsystem to the step-changes in S_e is illustrated in Fig. 12a, the operating voltage quickly stabilizes at 0.938 V, 0.776 V and 0.592 V corresponding to the three grid power steps of 0.3 MW, 0.8 MW and 1.3 MW. The fuel gas to power efficiency (Fig. 12b) decreases from 0.556 to 0.385 at the stepping conditions because the overpotentials are higher at lower operating voltage. The overall performance of SOFC operational mode is summarized in Table 6. A total 3999 MJ electricity from the Re-SOC (operating in SOFC mode) is supplied to the grid, achieving a 46.1% gas to power conversion efficiency. This conversion efficiency is comparable to other large-scale power generation solutions based on SOFC technologies (stationary applications), operating at an efficiency of around 50% [25,26]. Notably, the efficiency (for the Re-SOC system) is achieved under dynamic grid input conditions, during which the power generation density and the energy efficiency are traded off by customized valve control using effective control strategies. This architecture of the control strategy seems to be effective and can be further extended for more complicated reversible solid oxide cell system design.

4. Conclusions

This paper has proposed a combined system which integrates reversible solid oxide cells with CO_2 methanation process (ReSOC-MS) for the grid electricity storage at a scale of MW class. A dynamic model is developed to test the capability of ReSOC-MS for grid stabilization, supervised by a dynamic control strategy based on the system state (S_{H_2}) and grid state (S_e). Seven different operating modes: **M1**–**M7**, are mapped out at different (S_e, S_{H_2}) conditions to control the ReSOC subsystem and the two-staged methanation subsystem by means of controlling the gas supply and voltage, aimed at achieving a stable fuel utilization, extending storage capacity and buffering the filling of the H_2 storage tank. It is shown from the simulation results (of stationary tests) that the power to gas efficiency of the ReSOC-MS can be 85.34% when operated at stationary grid condition (2 MW, SOEC mode at 1.44 V) with a CH_4 yield of 0.97 mol s^{-1}, viz. 68.1% CO_2 conversion ratio for 1000 s operation. During SOFC mode with 1 MW of power, a gas to power efficiency of 46.95% for the ReSOC-MS system is achieved at 0.71 V. In the dynamic tests of SOEC mode, it is proved that the ReSOC-MS system can store the surplus grid electricity with a power to gas efficiency greater than 70% provided the gird surplus electricity is lower than 4 MW. The ratio of CH_4 production and H_2 production can be adjusted by the control strategy to extend the system capacity for grid electricity storage by refraining from storing a large volume of H_2. In the SOFC mode, the ReSOC-MS can still maintain the CH_4 production when the system state is at **M3** (an acceptable level of H_2 storage).

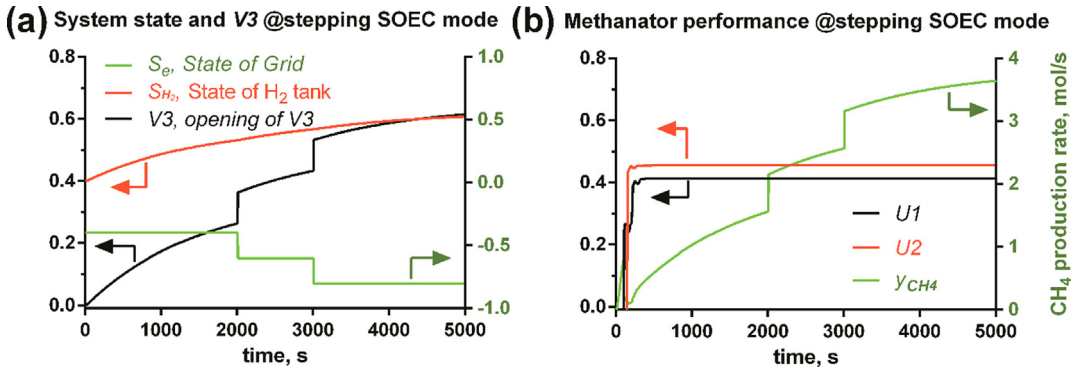

Fig. 9. (a) System state variables and (b) methanation system dynamic performance at stepping SOEC condition.

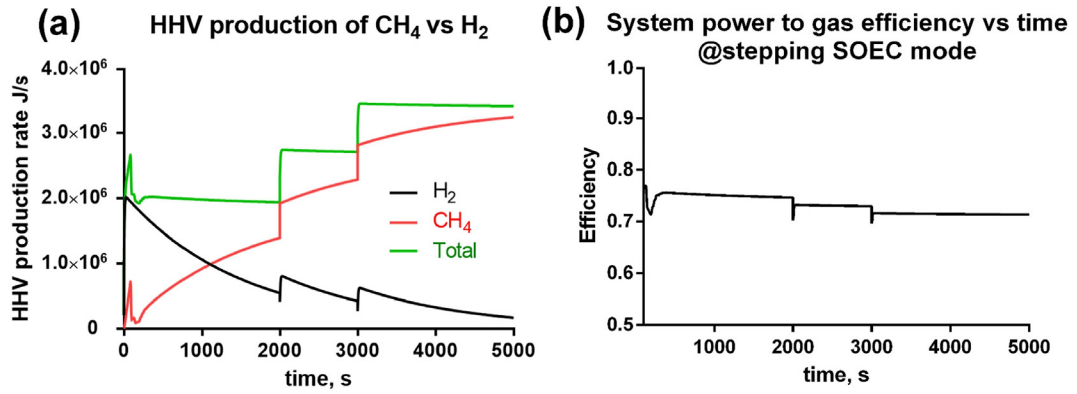

Fig. 10. (a) HHV of CH_4 and H_2 produced at the stepping SOEC condition; (b) the system power to gas efficiency at stepping SOEC condition.

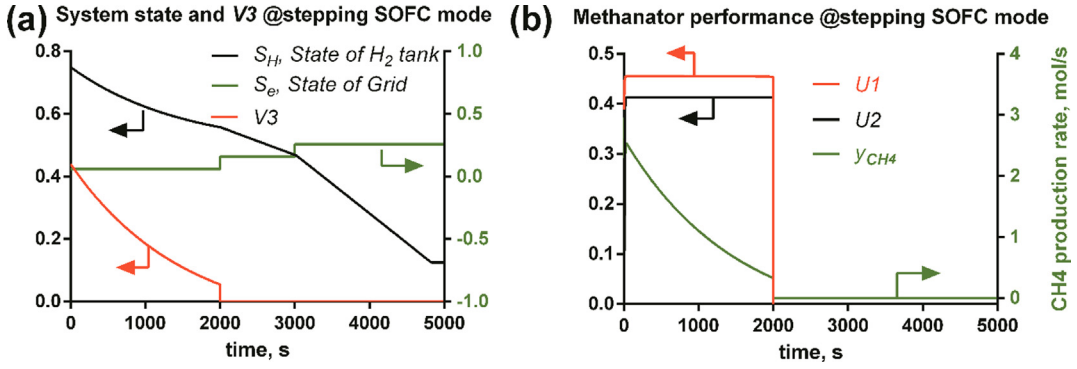

Fig. 11. (a) System state variables; (b) methanation system dynamic performance at stepping SOFC mode.

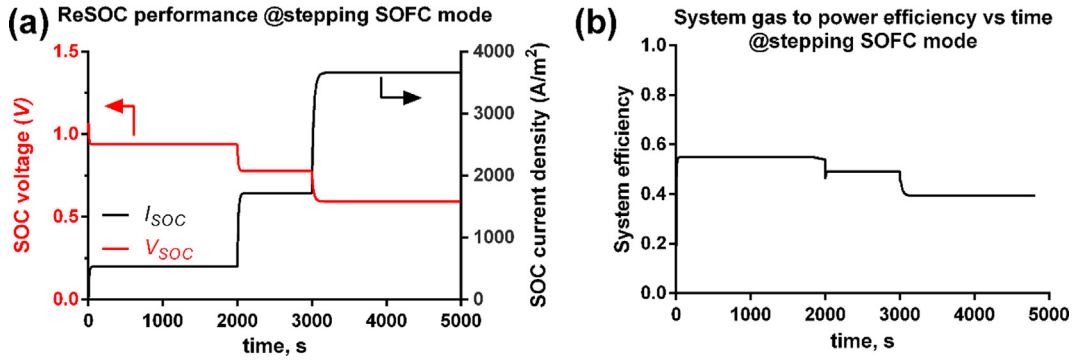

Fig. 12. (a) The current and voltage of ReSOC; (b) system gas to power efficiency dynamic performance at stepping SOFC mode.

Table 6
Summary of dynamic operation conditions and performance of the ReSOC-MS system in the SOFC case.

Performance parameters	Value
Stepping S_e input	0–2000 s: 0.06 (0.3 MW) 2000–3000 s: 0.16 (0.8 MW) 3000–5000 s: 0.26 (1.3 MW)
Operation time	5000 s
Initial H_2 tank state, S_{H_2}	0.75
Total grid power output, W_{g_SOFC}	3999 MJ
Total auxiliary power input, W_{aux_SOFC}	340.2 MJ
HHV value of H_2 consumption for SOFC, HHV_{H2_SOFC}	8366 MJ
Average system efficiency (gas to power)	46.1%
Operating voltage of ReSOC, V_{SOC}	0.938 V; 0.776 V; 0.592 V

Acknowledgments

This project has received funding from the European Union's Horizon 2020 research and innovation programme under grant agreement No. 731224. Disclaimer: the content of this document reflects only the author's view and the European Commission is not responsible for any use that may be made of the information it contains. The project is also supported by Natural Science Foundation of SZU (No. 2019087).

Appendix A. Supplementary material

Supplementary data to this article can be found online at https://doi.org/10.1016/j.apenergy.2019.04.162.

References

[1] European Union energy in figures statistical pocketbook 2017. Publications Office of the European Union; 2017.
[2] Eyer J, Corey G. Energy storage for the electricity grid: benefits and market potential assessment guide. Sandia Natl Lab 2010;20:5.
[3] Hittinger E, Whitacre JF, Apt J. What properties of grid energy storage are most valuable? J Power Sources 2012;206:436–49.
[4] Zabihian F, Fung A. A review on modeling of hybrid solid oxide fuel cell systems. Int J Eng 2009;3:85–119.
[5] Niaz S, Manzoor T, Pandith AH. Hydrogen storage: materials, methods and perspectives. Renew Sustain Energy Rev 2015;50:457–69.
[6] Jahangiri H, Bennett J, Mahjoubi P, Wilson K, Gu S. A review of advanced catalyst development for Fischer-Tropsch synthesis of hydrocarbons from biomass derived syngas. Catal Sci Technol 2014;4:2210–29.
[7] Jensen SH, Graves C, Mogensen M, Wendel C, Braun R, Hughes G, et al. Large-scale electricity storage utilizing reversible solid oxide cells combined with underground. Energy Environ Sci 2015;8:2471–9.
[8] Wendel CH, Kazempoor P, Braun RJ. Novel electrical energy storage system based on reversible solid oxide cells: system design and operating conditions. J Power Sources 2015;276:133–44.
[9] Rivera-Tinoco R, Farran M, Bouallou C, Auprêtre F, Valentin S, Millet P, et al. Investigation of power-to-methanol processes coupling electrolytic hydrogen production and catalytic CO_2 reduction. Int J Hydrogen Energy 2016;41:4546–59.
[10] Rönsch S, Schneider J, Matthischke S, Schlüter M, Götz M, Lefebvre J, et al. Review on methanation – from fundamentals to current projects. Fuel 2016;166:276–96.
[11] Ren J, Musyoka NM, Langmi HW, Mathe M, Liao S. Current research trends and perspectives on materials-based hydrogen storage solutions: a critical review. Int J Hydrogen Energy 2017;42:289–311.
[12] Chen B, Xu H, Zhang H, Tan P, Cai W, Ni M. A novel design of solid oxide electrolyser integrated with magnesium hydride bed for hydrogen generation and storage–a dynamic simulation study. Appl Energy 2017;200:260–72.
[13] Chan S, Low C, Ding O. Energy and exergy analysis of simple solid-oxide fuel-cell power systems. J Power Sources 2002;103:188–200.
[14] Mary N, Augustine C, Joseph S, Heartson S. Dynamic modeling and fuzzy control for solid oxide fuel cell (SOFC). Int J Adv Res Electr Electron Instrum Eng 2016;5:5488–97.
[15] Padulles J, Ault GW, Mcdonald JR. An integrated SOFC plant dynamic model for power systems simulation. J Power Sources 2000;86:495–500.
[16] Blackburn J, Reethof G, Shearer J. Fluid Power Control; 1960. USA: MIT Press. n.d.
[17] Gao Z, Mogni LV, Miller EC, Railsback JG, Barnett SA. A perspective on low-temperature solid oxide fuel cells. Energy Environ Sci 2016;9:1602–44.
[18] Schlereth D, Hinrichsen O. A fixed-bed reactor modeling study on the methanation of CO_2. Chem Eng Res Des 2014;92:702–12.
[19] Froment GF. Methane steam reforming, methanation and water-gas shift : 1. Intrinsic Kinetics 1989;35:88–96.
[20] Rostrup-Nielsen JR, Pedersen K, Sehested J. High temperature methanation. Sintering and structure sensitivity. Appl Catal A Gen 2007;330:134–8.
[21] Wagner W, Kretzschmar H-J. IAPWS industrial formulation 1997 for the thermodynamic properties of water and steam. Int Steam Tables Prop Water Steam Based Ind Formul IAPWS-IF97; 2008:7–150.
[22] Koschany F, Schlereth D, Hinrichsen O. On the kinetics of the methanation of carbon dioxide on coprecipitated $NiAl(O)_X$. Appl Catal B Environ 2016;181:504–16.
[23] Rönsch S, Köchermann J, Schneider J, Matthischke S. Global reaction kinetics of CO and CO_2 methanation for dynamic process modeling. Chem Eng Technol 2016;39:208–18.
[24] Wendel CH, Kazempoor P, Braun RJ. A thermodynamic approach for selecting operating conditions in the design of reversible solid oxide cell energy systems. J Power Sources 2016;301:93–104.
[25] Yi Y, Smith TP, Brouwer J, Rao AD, Samuelsen GS. Simulation of a 220 kW hybrid SOFC gas turbine system and data comparison. In: Electrochemical society proceedings volume 2003–07; 2003.
[26] Ando Y, Oozawa H, Mihara M, Irie H, Urashita Y, Ikegami T. Demonstration of SOFC-micro gas turbine (MGT) hybrid systems for commercialization. Mitsubishi Heavy Industr Tech Rev 2015;52(4).